

RESEARCH

Open Access



Aspergillus nidulans cell wall integrity kinase, MpkA, impacts cellular phenotypes that alter mycelial-material mechanical properties

Kelsey Gray¹, Harley Edwards¹, Alexander G. Doan¹, Walker Huso¹, JungHun Lee¹, Wanwei Pan¹, Nelanne Bolima¹, Meredith E. Morse¹, Sarah Yoda¹, Isha Gautam⁴, Steven D. Harris², Marc Zupan³, Tuo Wang⁴, Tagide deCarvalho⁵ and Mark R. Marten^{1*}

Abstract

Mycelial materials are an emerging, natural material made from filamentous fungi that have the potential to replace unsustainable materials used in numerous commercial applications (e.g., packaging, textiles, construction). Efforts to change the mechanical properties of mycelial-materials have typically involved altering growth medium, processing approaches, or fungal species. Although these efforts have shown varying levels of success, all approaches have shown there is a strong correlation between phenotype (of both fungal mycelia and mycelial material's assembly) and resultant mechanical properties. We hypothesize that genetic means can be used to generate specific fungal phenotypes, leading to mycelial materials with specific mechanical properties. To begin to test this hypothesis, we used a mutant of the model filamentous fungus, *Aspergillus nidulans*, with a deletion in the gene encoding the last kinase in the cell wall integrity (CWI) signaling pathway, *mpkA*. We generated one set of mycelial materials from the $\Delta mpkA$ deletion mutant (A1404), and another from its isogenic parent (A1405; control). When subjected to tensile testing, and compared to material generated from the control, $\Delta mpkA$ material has similar elastic modulus, but significantly increased ultimate tensile strength, and strain at failure. When subjected to a fragmentation assay (i.e., resistance to shear-stress), the $\Delta mpkA$ material also had higher relative mechanical strength. To determine possible causes for this behavior, we carried out a comprehensive set of phenotype assessments focused on: three-dimensional structure, hyphal morphology, hyphal growth behaviors, and conidial development. We found, compared to the control, material generated from the $\Delta mpkA$ mutant manifests significantly less development, a modified cell wall composition, larger diameter hyphae, more total biomass, higher water capacity and more densely packed material, which all appear to impact the altered mechanical properties.

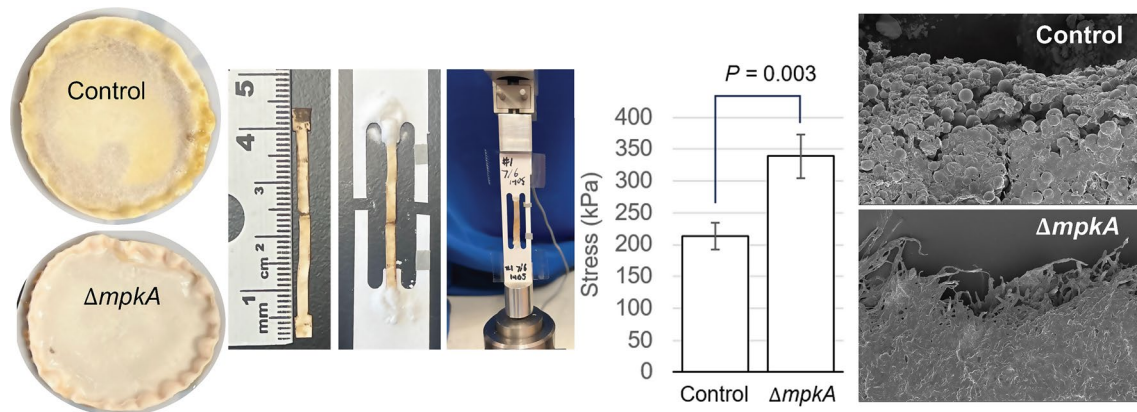
*Correspondence:
Mark R. Marten
marten@umbc.edu

Full list of author information is available at the end of the article



© The Author(s) 2024. **Open Access** This article is licensed under a Creative Commons Attribution-NonCommercial-NoDerivatives 4.0 International License, which permits any non-commercial use, sharing, distribution and reproduction in any medium or format, as long as you give appropriate credit to the original author(s) and the source, provide a link to the Creative Commons licence, and indicate if you modified the licensed material. You do not have permission under this licence to share adapted material derived from this article or parts of it. The images or other third party material in this article are included in the article's Creative Commons licence, unless indicated otherwise in a credit line to the material. If material is not included in the article's Creative Commons licence and your intended use is not permitted by statutory regulation or exceeds the permitted use, you will need to obtain permission directly from the copyright holder. To view a copy of this licence, visit <http://creativecommons.org/licenses/by-nc-nd/4.0/>.

Graphical Abstract



Introduction

An accumulation of societal pressures (e.g., increased world population, heightened consumer demand, depletion of non-renewable resources), has led to increased interest in developing sustainable materials [1–3]. Fully biobased materials have the potential to alleviate these pressures due to their 100% renewability and their ability to decompose naturally [1, 4, 5]. Furthermore, nature has already demonstrated its aptitude for producing materials that possess some of the most elite mechanical properties known to man (e.g., silk's strength rivals steel and Kevlar) [6]. Unlocking the full potential of various biobased materials will require a stronger understanding of how the composition, assembly, and growth behaviors of these materials impact resultant mechanical properties. Knowledge of these factors will allow manipulation of these traits to achieve specific and desirable mechanical properties [5].

Materials made out of filamentous fungi, or mycelial materials, represent one of the most promising fully-biobased materials available [7]. Mycelial materials have been championed due to their high mechanical strength, ability to be easily composted, inexpensive production costs, and tolerance to various environments [8, 9]. Mycelial materials are typically produced in one of two forms [10]. Composites consist of a fungal-substrate mixture (e.g., fungi and sawdust), while pure materials are made exclusively from fungi, typically grown in liquid medium. In both cases, the specific species or strain of the fungus used contributes significantly to the resultant material's mechanical properties [9, 11]. Composite mycelial materials offer both advantages and disadvantages related to the mechanical properties of the substrates used [12]. In contrast, pure mycelial materials offer the advantage of increased freedom in how they can be produced and utilized [13]. This freedom stems from the pure mycelial material's independence of other substances that can

influence cost, application limitations, mechanical properties, and other aspects that impact pure mycelial materials usefulness [13].

As a result of this flexibility, pure mycelial materials are being used, or considered, for a broad range of applications. For example, they are already being used as replacements for foam and leather and may eventually replace polystyrene packaging in addition to being used as support material for electronics [13]. There is also potential for pure mycelial materials to take on identities as building materials (e.g., sound and heat insulation), nanopapers [12, 14], and engineered living materials [15]. However, for a number of applications, the mechanical demands exceed the capacity of pure mycelial materials, and thus there is a need for improvement in mycelial material mechanical properties [13, 16]. Past reports of improvements in the mechanical properties of pure mycelial materials (e.g., *Ganoderma lucidum* or *Pleurotus ostreatus*) have typically involved changing growth medium [17]. Others have treated mycelial materials with plasticizers, increasing the material's elasticity, but reducing its ultimate tensile strength [18, 19]. An exciting opportunity to modify the mechanical properties of mycelial materials lies in genetic manipulation of the fungi involved. However, few reports exist using this approach [20, 21].

Two recent studies have explored the idea of evaluating fungal phenotypes as drivers for differences in mechanical properties of resultant mycelial materials [17, 21]. In these studies, scanning electron microscopy (SEM) was used to characterize mycelial-material packing density and surface morphology [17, 21]. Atomic force microscopy (AFM) was used to characterize the dimensions of hyphae in the z-axis, in addition to mechanically testing mycelial materials on a microscale [17, 21]. FTIR was used for collecting data regarding the chemical composition of each fungus tested [17, 21]. The information

gathered through these assessments implied a strong connection between the measured phenotypes and resultant material mechanical properties.

While some phenotype-material connections have been made, it has been suggested that more robust characterization of fungal phenotypes (e.g., improved understanding of morphologies), and how they impact material mechanical properties, is required to fully realize the potential of mycelial materials [13, 16]. To this end, our overarching hypothesis is that genetic means can be used to rationally tune fungal phenotype, resulting in mycelial materials with specific mechanical properties. To begin to test this hypothesis, we used a mutant of the model fungus *Aspergillus nidulans* with a deletion in the gene encoding the last kinase in the cell wall integrity (CWI) signaling pathway, *mpkA*. The CWI pathway is responsible for cell wall integrity and repair [22] and is highly conserved in the fungal kingdom [23]. Deletion of *mpkA* ($\Delta mpkA$) renders the CWI pathway inoperative [24], and leads to significant morphological and growth defects [25]. Accordingly, we initially hypothesized that an inoperative CWI pathway would lead to weaker-walled hyphae and result in mycelial material with reduced ultimate tensile strength. To test this hypothesis, we grew mycelial materials from both the $\Delta mpkA$ mutant and its isogenic parent (control). We characterized the mechanical properties of the resultant mycelial material and found the $\Delta mpkA$ mutant produces material with increased ultimate tensile strength, strain at failure, and resistance to shear-stress. To understand why this occurs, we carried out an extensive set of assessments to better understand how this deletion impacts the phenotype of the mutant, and its corresponding material.

Materials and methods

Fungal strains and growth media

All experiments were carried out using a mutant containing an *mpkA* deletion ($\Delta mpkA$; FGSC 1404; *pyrG*^{AF} used to replace *mpkA*) and an isogenic control (FGSC 1405; *pyrG* transformed back into SO451) [26] obtained from the Fungal Genetic Stock Center (FGSC, Manhattan, KS) [27]. Both genotypes were generated from the SO451 background (*pyrG89*; *wA3*; *argB2*; $\Delta nkuAku70::argB pyrO4$; *sE15 nirA14 chaA1 fwA1*) [28]. Both the $\Delta mpkA$ mutant and the control were first cultivated on modified MAG-V agar plates. Modified MAG-V agar contained 2 g/L BD Bacto Peptone, 1 mL/L vitamin solution, 1 mL/L Hutner's trace elements solution, 20 g/L granulated agar, 1.12 g/L uracil, 1.22 g/L uridine, 35.065 g/L NaCl, 20 g/L glucose, and 20 g/L malt extract. The trace element solution was made of: 22 g/L ZnSO₄·7H₂O, 11 g/L H₃BO₃, 5 g/L MnCl₂·4H₂O, 5 g/L FeSO₄·7H₂O, 1.7 g/L CoCl₂·6H₂O, 1.6 g/L CuSO₄·5H₂O, 1.5 g/L Na₂MoO₄·2H₂O and 50 g/L EDTA (Na₄). The vitamin

solution contained: 100 mg/L biotin, 100 mg/L pyridoxine, 100 mg/L thiamine, 100 mg/L riboflavin, 100 mg/L p-aminobenzoic acid, and 100 mg/L nicotinic acid [29, 30]. Modified YGV used to grow mycelial materials contained 1 g/L yeast extract, 2 g/L BD Bacto peptone, 1 g/L Bacto casamino acids, 1 mL/L vitamin solution, 1 mL/L Hutner's trace elements solution, 44.21 g/L KCl, 1.12 g/L uracil, 1.22 g/L uridine, 20 g/L glucose, 20 g/L malt extract, 10 g/L proline, 50 mL/L nitrate salts, and 5 mL/L MgSO₄ solution. The nitrate salts are made from 142.7 g/L KNO₃, 10.4 g/L KCl, 16.3 g/L KH₂PO₄, and 20.9 g/L K₂HPO₄. The MgSO₄ solution calls for 104 g/L of MgSO₄.

Growing mycelial materials

The $\Delta mpkA$ mutant and the control were first grown on separate modified MAG-V plates for 5 days. Conidia from resulting conidial lawns were harvested using 5 mL of sterile DI water and a glass pipette. The harvested conidial suspension was placed into a conical tube, counted and diluted to the concentration of 8×10^6 conidia/mL using modified YGV. The conical tube containing both the modified YGV and the conidia was vortexed, and 7.5 mL of the homogenized YGV- conidia mixture was added to a single 60×15 mm petri dish (Fisherbrand) to generate one mycelial material "disk." This process was repeated to produce additional mycelial material disks. The filled petri dishes were placed into an incubator for 120 h at 28°C. The mycelial material formed on the top layer of liquid in each plate. Mycelial materials were harvested by transferring the entire contents of the petri dish to a beaker filled with diluted bleach, and then washed with DI water.

Growth curve

To develop growth curves, 20 mycelial material petri dishes were prepared (Sect. 2.2) for both the control and the $\Delta mpkA$ mutant. At each time point, the entire contents of two petri dishes for each strain were recovered via vacuum filtration (60 mm filter paper disk) and dried at 60°C until they reached constant weight. The average dry biomass of the two values at each time point was used to generate the growth curve.

Tensile testing

Tensile testing was carried out on nominal 4×40 mm coupons cut (Universal Laser Systems VLS 3.6/6) from mycelial disks. At minimum, five coupons were cut from each disk (three disks per genotype). Before testing, coupons were hydrated in a 40:60 glycerol: water mixture for 1 min [31], coated in petroleum jelly [32], and dried with warm air for approximately 1 min on each side. Coupon dimensions were then precisely measured using a dissection microscope (Leica Microscope s9i Model meb115),

and adhered to a paper frame (for stability) using cyanoacrylate adhesive (Loctite) and NaHCO_3 powder (to accelerate drying [33]). The frame was mounted to the tensile testing device (Instron 3369) with double sided tape. Immediately prior to testing, the paper frame was cut on each side so only mycelial material was tensile tested. Two pieces of reflective tape were placed onto the paper frame to enable laser extensometer (Electronic Instrument Research Model LE-01) strain measurement during applied stress. Measured dimensions of the coupon were entered into the tensile testing software (Instron Bluehill lite) prior to each test to calculate the stress obtained through a sensor (Transducer Techniques Sensor) connected to the tensile testing device. All tests were stopped manually after material failure. The maximum stress and strain values were identified as the ultimate tensile strength and strain at failure, respectively. The Young's Modulus was calculated by measuring the linear slope of the stress (y-axis) and strain (x-axis).

Mycelial structure and hyphal morphology

For scanning electron microscopy (SEM) sample prep, fractured tensile-tested mycelial materials were removed from the paper frame, adhered to an aluminum stub using double sided carbon tape, sputter coated (Cressington 108 Manual Sputter Coater - Au/Pd target), and imaged using an FEI Nova NanoSEM 450. For transmission electron microscopy (TEM) sample prep, two mycelial disks from each genotype were cut into 1×1 cm squares and placed into a scintillation vial overnight at 4°C . Vials were filled with a solution of 2% paraformaldehyde, 2.5% glutaraldehyde, in 0.1 M sodium cacodylate buffer at 7.4 pH. Samples were washed and submerged with fresh 0.1 M sodium cacodylate buffer, while being gently mixed for 10 min; this step was repeated twice. Samples were gently mixed in 0.1 M sodium cacodylate buffer and 50 mM glycine for 15 min. Samples were again washed and mixed with 0.1 M sodium cacodylate buffer for 10 min, three different times. Washed samples were incubated in 0.1 M sodium cacodylate buffer with 1% OsO_4 for 1–2 h, and rinsed with deionized water four times for 10 min each. The mycelial material was put through a dehydration series where each step was repeated three times for 10 min. Samples were first submerged in 35% ETOH, then 50% ETOH, 70% ETOH with 1% uranyl acetate, 70% ETOH, 95% ETOH, 100% ETOH, and 100% Acetone. Afterwards, samples were placed in 2:1 Acetone/Epon for 1 h, then sectioned into 80 nm slices using an ultramicrotome (Leica Microsystems UC7) and imaged on a FEI Tecnai T12 TEM. The diameter of the hyphae and thickness of the cell wall were measured at three different points (on the hyphae) from the TEM images of 20 different hyphae per genotype using ImageJ software.

Hyphal resistance to fragmentation

The mycelial disks (one disk per trial, four trials per genotype) were placed into a high-shear mixer (Hamilton Beach Model #58615) with 370 mL of water. The first sample (20 mL) was removed after 5 s, and subsequent samples (20 mL) were removed at 10s intervals. After collection, each sample was subjected to a particle size analysis (Malvern Mastersizer 3000) to provide a relative measure of average particle size, reported as average diameter (μm), as we have described previously [34]. Specifically, taking the 90th percentile of the particle size distribution (PSD) has been found to be representative of hyphal size.

Cell wall composition

The composition of rigid and mobile components was determined by analyzing peak volumes in 2D ^{13}C - ^{13}C spectra, employing 53 ms CORD and DP refocused J-INADEQUATE schemes, respectively. Solid-state NMR spectra were collected on an 800 MHz Bruker Avance Neo NMR spectrometer using a 3.2 mm HCN magic-angle spinning probe. ^{13}C chemical shifts were calibrated on the tetramethylsilane (TMS) scale. Peak volumes were extracted using the integration function of Bruker Topspin software. To minimize uncertainties from spectral crowding, only well-resolved signals were considered for the compositional analysis. The identified NMR peaks, along with their resonance assignments and corresponding peak volumes, were visualized in a donut graph using Origin 2021.

Samples taken from four different disks per genotype were used to measure the percentage of melanin in a material. Mycelial materials were soaked in hexamethyldisilazane (HMDS) for 5 min, and air dried for at least 90 min (fume hood). The dried material was inserted into a cryogenic vial containing 3 glass beads (diameter 3 mm), and pulverized with a Mini Beadbeater (Biospec Products) at 5000 rpm for 1 min. A small amount of the pulverized mycelial material was massed on a balance (g), recorded, and used in a commercial assay (Amplite® Fluorimetric Melanin Assay Kit, AAT Bioquest) to quantify melanin mass (g). The percentage of melanin from the measured mycelial material was calculated by dividing the mass of the melanin derived from the commercial kit by the mass of the dried mycelial material previously measured and used in the kit.

Asexual development (conidiation)

Fungal lawns were grown using 200 μL of conidia solution with a concentration of 8×10^6 conidia/mL to inoculate modified MAG-V plates. Conidia from these lawns were harvested using the same approach mentioned in Sect. 2.2. A small aliquot of the conidial suspension was diluted by 1000x in water and 10 μL of the diluted

conidial suspension was placed into a hemocytometer (Fisher Scientific), so the number of conidia could be counted under an inverted microscope (Zeiss Axiovert 200).

Germination and total branching rate

Germination and total branching rates (the combined rate of hyphal germination and hyphal branching phenomena) were measured using a previously published protocol involving coverslips [25, 35]. Coverslips were sterilized while petri dishes filled with modified YGV media (without KCl) were placed into an incubator at 28 °C. Coverslips were submerged in Concanavalin A [35] for 20 min, rinsed with sterile DI water and dried under a flame for 1 h. After 1 h, conidia were harvested from plates using the same process mentioned in Sect. 2.2, deposited into the modified YGV media at a concentration of 1×10^5 conidia/mL, and added to each coverslip. Fresh 1 mL of conidial suspension was used for each coverslip. Coverslips were dried again under a flame for 1 h before being added to the incubating petri dish. A coverslip was removed at every hour, starting from hour 9 until hour 16, and fixed in 3% formaldehyde (Macron Fine Chemicals) for 30 min minimum. 30 images of clearly defined and isolated hyphae at each time point were captured at 40x with a fluorescent microscope (Zeiss Axiovert 200) using calcofluor white (CFW; Sigma-Aldrich) stained coverslips. The number of germination tubes and number of branches from each of the 30 images were measured and recorded using ImageJ.

FTIR spectroscopy

Samples for FTIR spectrometry were prepared by submerging a piece of mycelial material into 40:60 volume based glycerol: water mixture for 60 s and blotting the surface dry. One sample was inserted into the FTIR at a time, and scanned four times in the 4000 cm^{-1} to 650 cm^{-1} range using transmission mode in the FTIR software (PerkinElmer Spectrum). The peaks from the

FTIR readings were analyzed via an infrared spectroscopy tables found in the literature [36].

Significance testing

All quantitative data was subjected to T-tests to identify any significant differences between groups using Microsoft Excel.

Results and discussion

Mycelial material growth

For all assessments, mycelial materials were generated identically for the control (A1405) and the *mpkA* deletion mutant ($\Delta mpkA$; A1404). The mycelial materials were grown as disks (Fig. 1A, B), on the surface of static liquid growth medium at 28 °C for 120 h. Compared to the control, the $\Delta mpkA$ mutant produced thinner, wetter-looking, material with less surface texture (Fig. 1B). Figure 1C shows growth curves (measured as average total biomass) during the formation of the mycelial disks, over a span of 120 h. For the first 75 h, the control material grew exponentially at a rate of 0.041 h^{-1} while the $\Delta mpkA$ material grew at a rate of 0.043 h^{-1} , with no significant difference between the two ($P=0.84$). The material generated from the control stops increasing in mass after approximately 100 h, but the $\Delta mpkA$ mutant material continued to increase in mass for 120 h, leading to 50% more biomass ($P=0.001$), as shown in Fig. 1C.

Tensile testing, mechanical properties, and fracture analysis

After 120 h of growth, mycelial materials were carefully removed from the surface of the liquid growth medium (prepared as described in the Methods section) and subjected to tensile testing. Figure 2A shows the strips used for testing, the paper frame on which the strips were mounted (Fig. 2B), and one of these frames loaded onto the tensile testing apparatus (Fig. 2C). Typical tensile-test curves for the control and $\Delta mpkA$ materials are shown in Fig. 2D and E, where legend numbers indicate relative

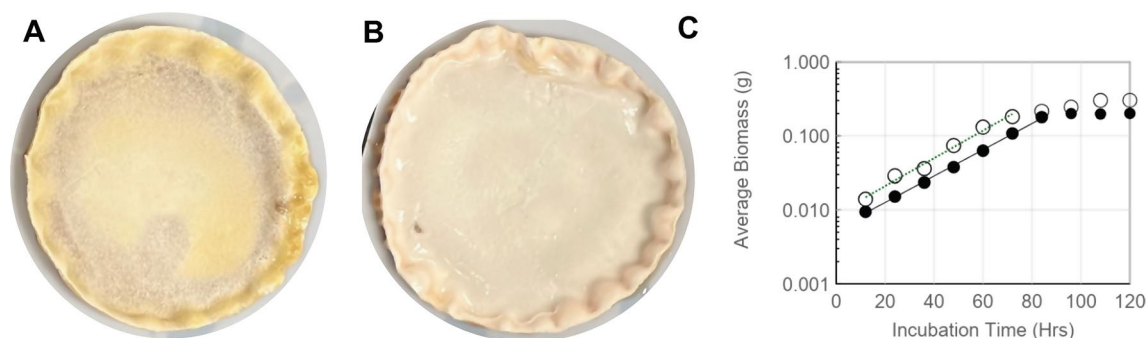


Fig. 1 Mycelial material generation. Mycelial discs were grown from the (A) control (A1405) and (B) $\Delta mpkA$ (A1404) fungal strains. (C) Average dry material biomass (g) from two disks for the control (●) and $\Delta mpkA$ (○) increased exponentially, with average specific growth rates (straight lines) of 0.041 h^{-1} and 0.043 h^{-1} and final biomass values of 0.20 g and 0.30 g respectively. No significant difference in growth rates ($P=0.84$); significant difference in final weights ($P=0.001$)

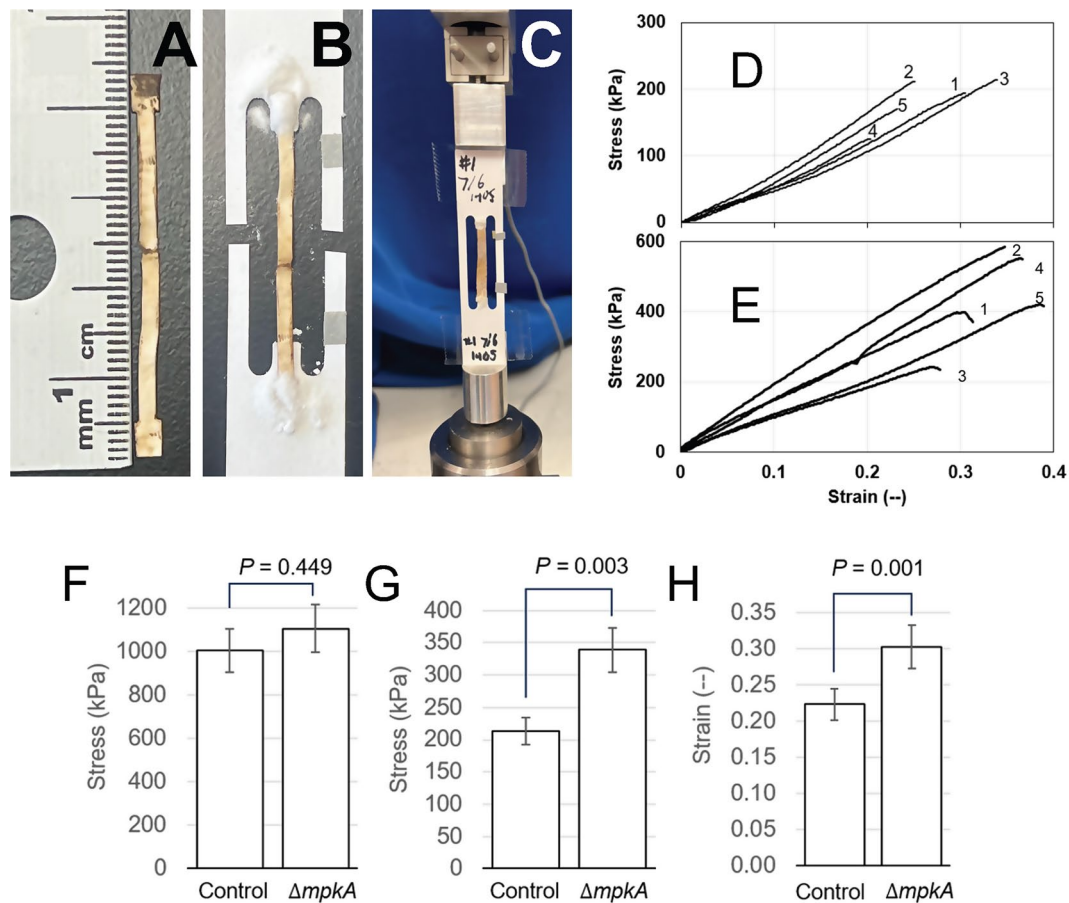


Fig. 2 Tensile testing of mycelial material. Material discs were dried and then (A) cut into strips, which were (B) mounted in a paper frame which was then (C) mounted on load-frame for testing. Details in Methods. Typical stress-strain curves for mycelial material generated from the (D) control (A1405) and (E) $\Delta mpkA$ (A1404) fungal mutant. In both cases, five test strips were cut from the center of a single disc of mycelial material. Numbers on each graph indicate the relative position of where coupons (panel A) were cut from the mycelial material. Positions 1–5 were immediately adjacent to each other, with position 3 in the middle of the material disk. For both fungal genotypes, the material shows linear elasticity before failure. Mechanical properties determined from stress-strain testing ($n=15$) of material generated from control (A1405) and $\Delta mpkA$ (A1404) mutant. (F) Average Young's modulus, (G) ultimate tensile strength and (H) strain at failure

position of tested coupons. All tensile testing showed only random variation with regard to position, implying material was homogeneous with regard to material properties. For both genotypes, materials showed only linear elasticity before failure, a characteristic of brittle materials [37]. Data collected from the tensile test were used to determine: Young's modulus (YM), ultimate tensile strength (UTS) and strain at failure (SF). Average values for these properties ($n=15$ per genotype) are shown in Fig. 2F-H. While both the control and the $\Delta mpkA$ material had similar YM ($P=0.449$), material generated from the $\Delta mpkA$ mutant had significantly higher values of UTS ($P=0.003$) and SF ($P=0.001$) at 339 ± 18 kPa and 0.30 ± 0.02 respectively compared to the control which had a UTS of 213 ± 33 kPa and a SF at 0.22 ± 0.01 . These results imply that the $\Delta mpkA$ material is stronger and more elastic than the control material.

Surface morphology, fracture analysis, and internal morphology

To help understand the results from tensile testing, we used scanning electron microscopy (SEM) to analyze material surface morphology and morphology at the point of fracture. This allowed observation of the material's three-dimensional structure, which was assessed for the degree of density (e.g. presence and/or size of void, hyphal packing) and morphological features. In general, compared to the control, we found the $\Delta mpkA$ material appeared to have (i) fewer developmental structures (i.e. conidia and Hülle cells.) and (ii) a more densely packed morphology with fewer visible voids (Fig. 3A, C). Similarly, the fracture point of the $\Delta mpkA$ material showed relatively more hyphae and fewer developmental structures (Fig. 3B, D). A previous study has shown that higher material density is correlated with increased mechanical strength [21], and the same appears to be true here. We suspect the lack of voids limits the number of

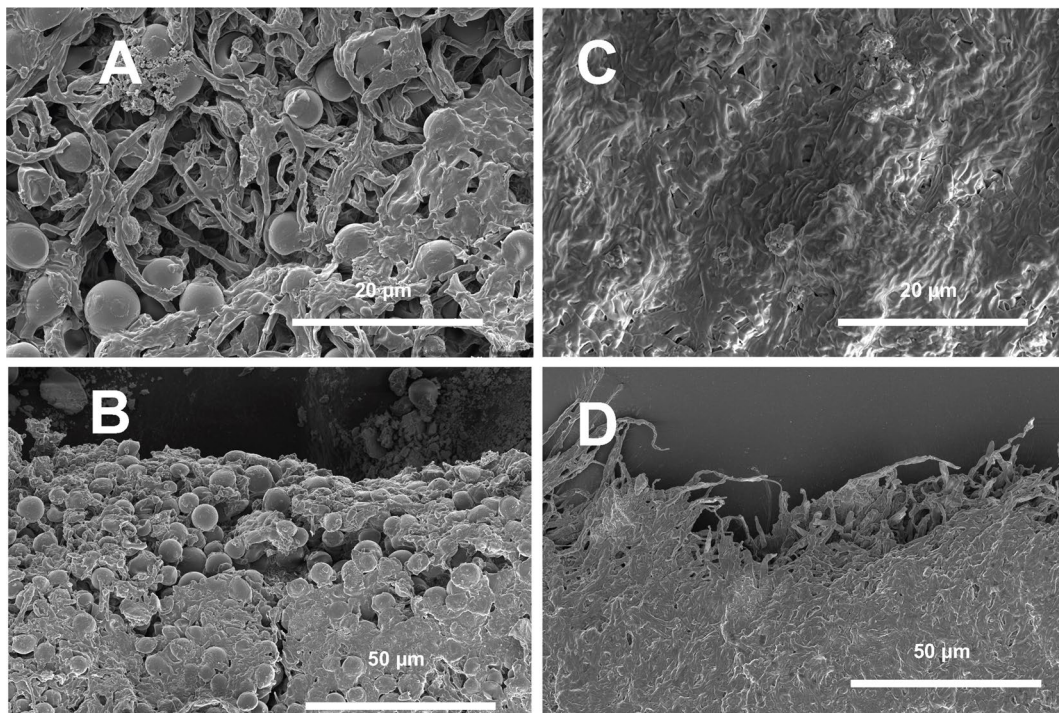


Fig. 3 Representative SEM images of mycelial material three-dimensional structure and morphological features. **(A)** Control (A1405) sample surface showing an abundance of developmental structures (e.g., conidia, Hülle cells), loose packing of hyphae, and voids in the material. **(B)** Fracture point of the same control sample. **(C)** The $\Delta mpkA$ (A1404) sample surface shows fewer developmental structures, denser hyphal packing, and an absence of voids. **(D)** Fracture point of the same $\Delta mpkA$ sample

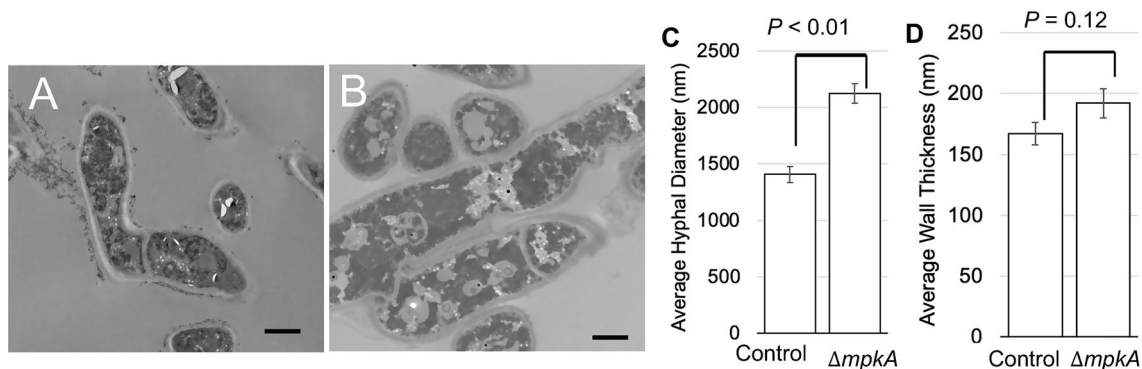


Fig. 4 Representative TEM images showing the hyphal morphology of **(A)** control (A1405) and **(B)** $\Delta mpkA$ (A1404) mutant. Size bars = 1 μ m. Measurements of hyphal morphology show that the **(C)** average hyphal diameter (nm) is significantly wider in the mutant and **(D)** cell wall thickness (nm) is similar

unsupported positions that could potentially weaken the material.

To assess internal hyphal morphology, samples ($n=20$ per genotype) from both the control and the $\Delta mpkA$ mutant were analyzed via transmission electron microscopy (TEM, Fig. 4). From these images, hyphal cross-sections were used to determine average hyphal diameter (Fig. 4C) and the average cell wall thickness (Fig. 4D). We hypothesize that mycelial materials with larger hyphal diameters and thicker cell walls would be more equipped to handle larger forces, resulting in stronger materials. Compared to the control, $\Delta mpkA$ mutant hyphae showed

a 50% larger hyphal diameter at 2124 ± 86 nm compared to a hyphal diameter of 1405 ± 70 nm in the control ($P < 0.01$); there was no significant difference in cell wall thickness.

Shear stress tolerance and specific fragmentation rate

To assess relative material strength, we used a fragmentation assay that we have described previously for fungi grown in suspension culture [34]. To carry out this assay fungal mycelia are removed from their growth environment, suspended in liquid, and are exposed to high shear-stress. This causes the mycelial hyphae to fragment over

a relatively short period of time (1 min). Measurements of decreasing mycelial size over this short period (e.g., every 5 s) are used to determine specific fragmentation rate, which is inversely proportional to the strength of the fungal cell walls [38] (i.e., stronger hyphae fragment more slowly). In this study, we carried out a similar assay, but added an entire disc of mycelial material to DI water, and subjected the material to high-shear mixing (Fig. 7). In this case, we added an entire disc of mycelial material to DI water, and subjected the material to high-shear mixing (Fig. 5). The fragmentation process in the high-shear mixer has two phases: (i) the initial cutting phase and (ii) the cavitation fragmentation phase [39]. The first phase occurs quickly (≤ 5 s) as the blades of the high-shear mixer accelerate from rest. During the initial mixing of the material, we assume that some mechanical shearing occurred without the presence of cavitation forces - implying the material's tolerance to mechanical shear stress [40]. Figure 5B shows the $\Delta mpkA$ mutant has a significantly larger size after this first phase at 2231 ± 46 nm compared to 1794 ± 12 nm in the control ($P=0.02$). This finding is consistent with the finding of higher ultimate tensile strength for the $\Delta mpkA$ material. During the second phase, the mycelia themselves are breaking, and the slope of the curve can be used to determine specific fragmentation rate ($\mu\text{m/s}$) [34], where there is no significant difference between the two materials (Fig. 5C).

Cell wall composition

The filamentous fungal cell wall is essential for survival, providing protection from environmental, chemical, and mechanical stress. This structure is primarily composed of polysaccharides and melanin [22]. Within the mycelial cell wall of *Aspergillus* species, chitin physically associates with α -1,3-glucan and β -1,3-glucan to form

rigid core structures, which are embedded within a soft, hydrated matrix composed of β -glucans with various linkages [41], including β -1,3, β -1,3/1,6, and β -1,3/1,4-linkages. This composite structure is further enveloped by an outer layer enriched with proteins, galactomannan, and galactosaminogalactan. Some of the polysaccharides are covalently bonded, such as chitin- β -1,3-glucan-galactomannan and chitin- β -1,3-glucan, thereby conferring resistance to alkali extraction [42].

To assess the cell wall composition of materials generated with both the control and $\Delta mpkA$ mutant, we used a high-resolution, solid-state NMR approach as has been described previously [43]. The results are shown in Figs. 6 and 7. The 2D ^{13}C - ^{13}C CORD experiment, which probes the rigid core of the fungal cell wall, revealed that it is composed of α -1,3-glucan, β -1,3-glucan, chitin and chitosan (Fig. 6A, B), consistent with the results reported in recent studies [44, 45]. The compositional analysis shows a significant decrease ($P<0.05$) in α -1,3-glucan components in the $\Delta mpkA$ mutant (Fig. 6A-C), alongside a significant increase in the β -1,3glucan ($P<0.05$). Notably, no major changes were observed in the proportion of chitin and chitosan. In addition, employing 2D ^{13}C - ^{13}C DP J INADEQUATE experiment, probed the mobile domain of the cell wall. We observed the alternation of galactomannan structure with selectively increased amount of α -1,2-mannose. Interestingly, the $\Delta mpkA$ mutant exhibited GalNAc ($P<0.05$), monomer of galactosaminogalactan (GAG) linkages at 101 ppm and 55 ppm which was absent in positive control. This may suggest the compensatory mechanism for the loss of α -1,3-glucan, which is crucial for aggregation and biofilm formation. Previous studies have shown that both α -glucan and GAG play a significant role in hyphal aggregation [46]. Our observations also indicate a significant loss of galactose ($P<0.05$)

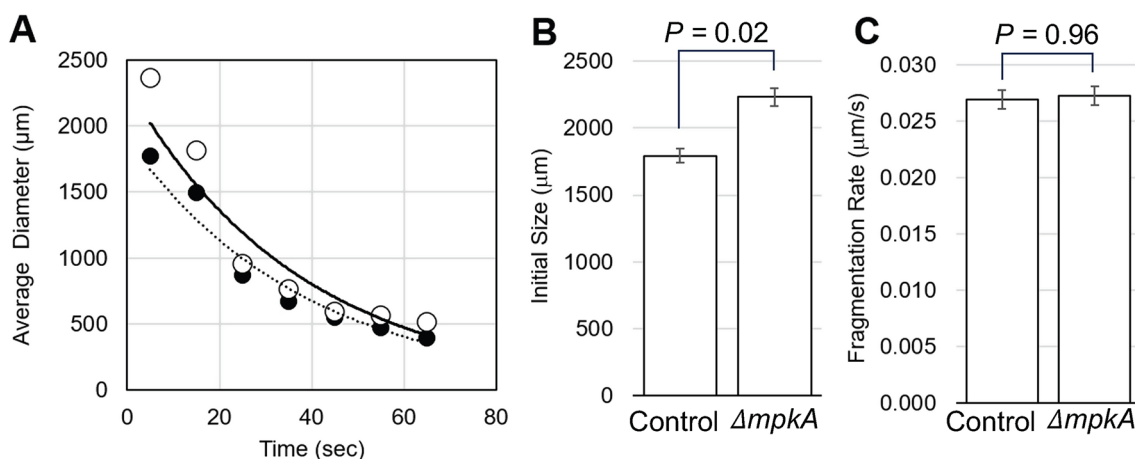


Fig. 5 Relative material strength measured in a high-shear mixer. **(A)** Average size ($n=4$) of fungal elements versus time in the high-shear mixer for material from the control (●) and $\Delta mpkA$ (○) mutant. Lines indicate exponential fit used to determine specific fragmentation rate. **(B)** Average size of fungal elements for the control and $\Delta mpkA$ mycelial material after 5s of high-shear mixing are significantly different ($P=0.02$). **(C)** Fragmentation rate, determined from exponential fits in A, are not significantly different ($P=0.96$)

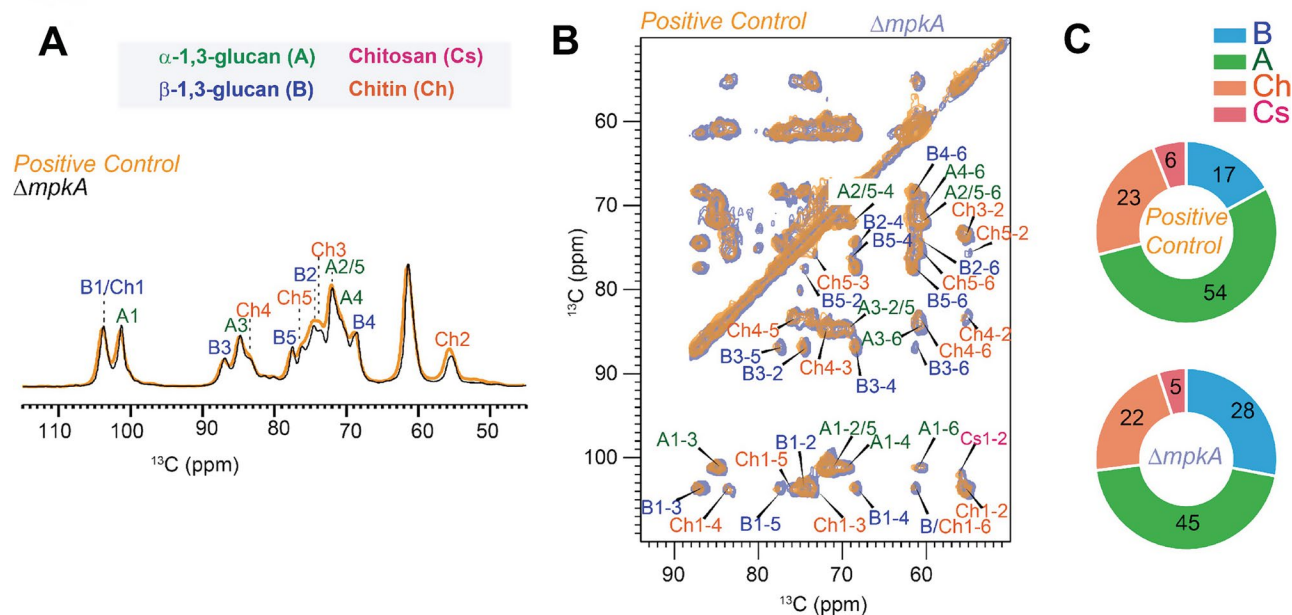


Fig. 6 Composition of rigid polysaccharide probed by high-resolution ssNMR. **(A)** Overlay CP spectra of positive control and $\Delta mpkA$ mutant, with the rigid polysaccharide shown in orange and black spectra. The glucan types and its carbon numbers are abbreviated, and color coded as: α -1,3-glucan (A, green), (β -1,3-glucan (B, blue), chitin (Ch, orange), chitosan (Cs, pink). **(B)** The 2D ^{13}C - ^{13}C CORD, correlation explores the spatial arrangement of cross-linkages among α -1,3-glucan, β -1,3-glucan, chitin, and chitosan. **(C)** The molar composition of these rigid components is determined by analyzing the peak volumes in the 2D ^{13}C - ^{13}C CORD spectra

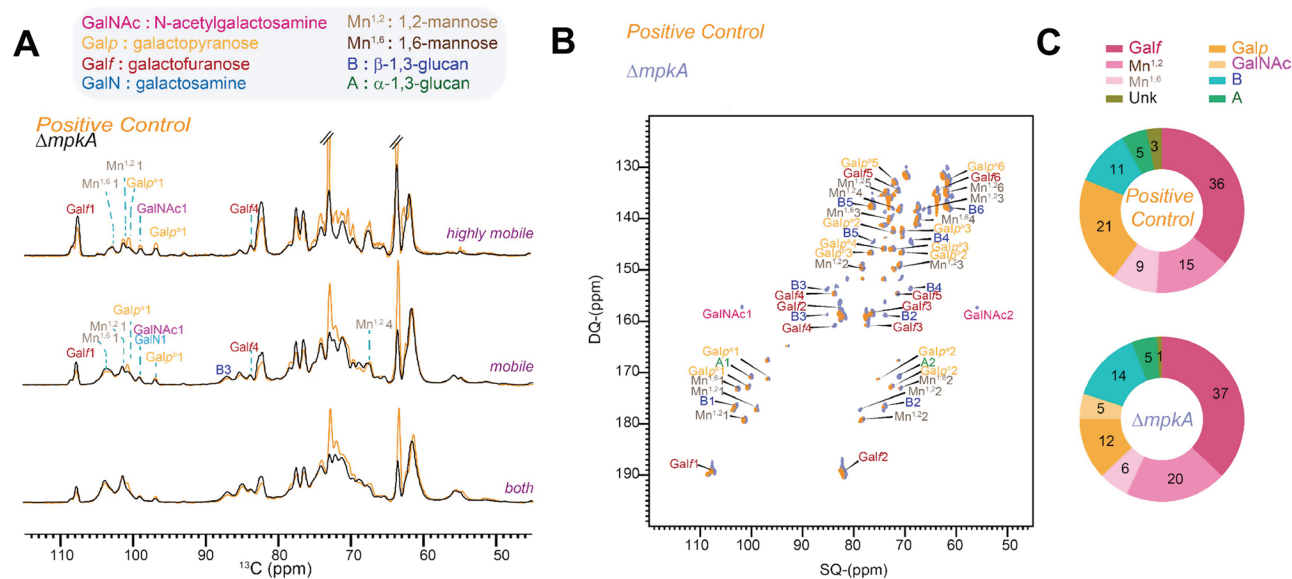


Fig. 7 Composition of mobile carbohydrates. **(A)** Overlay of 1D spectra for the control (A1405) and $\Delta mpkA$ mutant (A1404), shown in orange and black, representing the highly mobile region, semi-dynamic region, and cumulative region using INEPT, 2s DP, and 35s DP experiments. The glucan types, their monomers, and carbon numbers are labeled and color-coded as follows: galactofuranose (Galf, pink), α -1,2-mannose (Mn^{1,2}, light brown), α -1,6-mannose (Mn^{1,6}, brown), galactopyranose (Galp, yellow), and N-acetyl galactosamine (GalNAc, magenta). **(B)** The through-bond correlations 2D ^{13}C - ^{13}C -DP J INADEQUATE correlation spectrum, shown in orange and grey for positive control and mutant. **(C)** The molar composition of these mobile components determined by analyzing the peak volumes in the 2D DP-INADEQUATE spectra. The GM molecules are color-coded in pink shades, while the GAG components are shaded in orange in the donut graph. The legend corresponds to the abbreviations, linking the monomers to their assignments in the INADEQUATE spectra

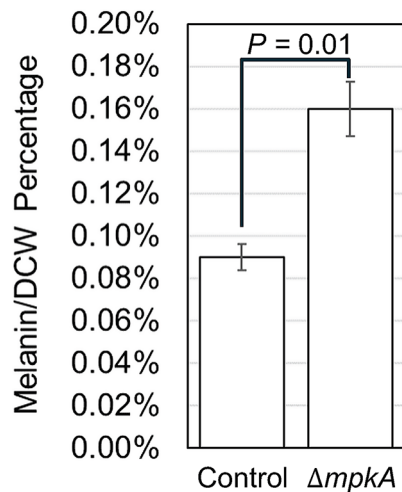


Fig. 8 Cell wall melanin content. Compared to the control, the $\Delta mpkA$ mutant produces significantly more (~80%) melanin ($P=0.01$)

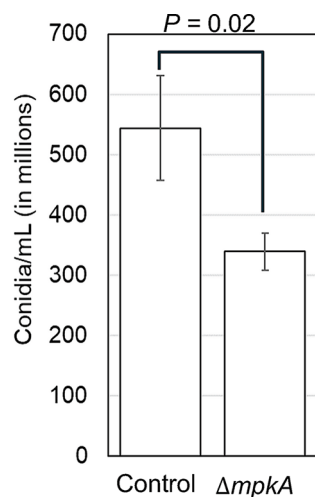


Fig. 9 Conidia collected, show that compared to the control, the $\Delta mpkA$ produces significantly fewer (40%) conidia ($P=0.02$)

in the mutant in comparison to positive control strain, which coincides with the appearance of GalNAc found only in the $\Delta mpkA$ mutant.

Melanin plays a role in preserving and hardening the fungal cell wall. Here, the percentage of melanin found in the cell wall was determined using a commercial assay ($n=4$ per genotype, Fig. 8). Compared to the control, material generated from the $\Delta mpkA$ mutant contained nearly twice the amount of melanin ($P=0.02$) per dry cell weight (DCW) at $0.16 \pm 0.01\%$ compared to the control which had $0.09 \pm 0.01\%$ melanin per DCW (Fig. 8).

Asexual development

The mechanical properties of mycelial materials are dependent on the interaction of hyphae within a grown material [13, 47, 48]. Hyphae extend and develop during vegetative growth, which is interrupted by asexual

development [49–51]. We hypothesize that more time for vegetative growth will lead to altered mechanical properties. SEM observations of the two genotypes used here implies that material generated by the $\Delta mpkA$ mutant contains fewer developmental structures (Fig. 3C). To better understand the extent of this phenomena, lawns of both the control and the mutant were grown on the surface of agar plates. Conidia from each genotype were collected and counted, and results are shown in Fig. 9. Figure 9 shows that the $\Delta mpkA$ mutant produced 40% less conidia than the control at $339 \times 10^6 \pm 12 \times 10^6$ conidia/mL compared to the control's $544 \times 10^6 \pm 34 \times 10^6$ conidia/mL ($P=0.02$).

Germination, and total branching rates

As previously stated, the mechanical properties of mycelial materials are dependent on the interaction of hyphae within a grown material [13, 47, 48]. Germination and branching rates are types of hyphal interactions found within a mycelial material. We hypothesize that altered rates of these phenotypes may lead to altered mechanical properties. To determine if there was a difference between the germination and branching rates of the two stains, we grew cells on cover slips as described previously [35]. This allows visualization of individual spores that develop into hyphae, thus allowing determination of germination and total branching rates. The control and $\Delta mpkA$ mutant ($n=30$ per genotype) displayed similar germination rates at 0.10 ± 0.02 germinated hyphae/hr and similar total branching rates at 0.11 ± 0.02 total branches/hr. The p value for each phenotype, germination rate ($P=0.46$) and total branching rate ($P=0.52$) indicates that there is no significant difference in either germination or total branching rates between the control and $\Delta mpkA$ mutant.

FTIR results

Testing via fourier transform infrared (FTIR) spectroscopy provides the ability to characterize the water content of heterogenous natural materials, and others have used this approach to characterize mycelial materials [17, 36]. In particular, FTIR is able to identify water found in a material through OH bonds, which are detected in the wavelength range from 3600 cm^{-1} to 3200 cm^{-1} [52, 53]. Figure 10 shows typical FTIR traces for the $\Delta mpkA$ mutant and the control, with a clear difference for the peaks within the wavelengths 3600 cm^{-1} to 3200 cm^{-1} . This height difference indicates a noticeable increase in the volume of water found in the $\Delta mpkA$ mutant compared to the amount of water found in the control. This finding is consistent with results from a previous study [21], in which the mutant with higher ultimate tensile strength and strain at failure, also contained more water, implying a correlation between increased water capacity

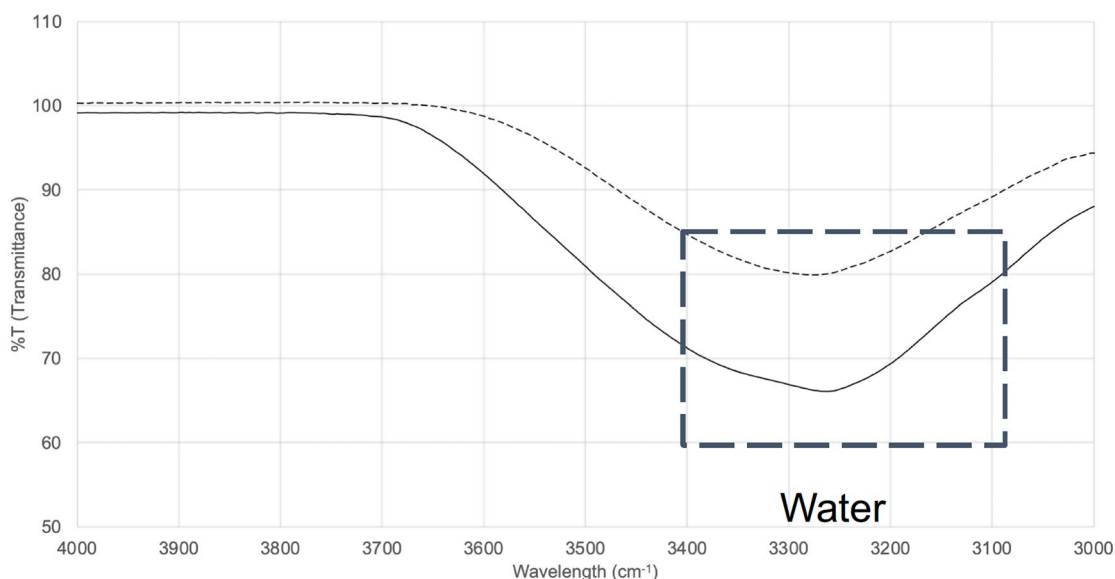


Fig. 10 FTIR traces for material grown from control (---) and $\Delta mpkA$ (—) mycelial materials. Annotated graph showing the difference in water between the control and the $\Delta mpkA$ mutant with a close up image highlighting additional traces. This graph also suggests that there might be additional chemical differences found between the control and the $\Delta mpkA$ mutant

and increased ultimate tensile strength and strain at failure.

Conclusion

We found deletion of the *A. nidulans mpkA* gene leads to mycelial materials with higher ultimate tensile strength, strain at failure, and resistance to shear-stress. This result was obtained through tensile testing of the actual material, and agrees with our findings regarding material behavior in a novel fragmentation assay [34].

To determine possible causes for this behavior, we characterized a number of different phenotypes for both the individual fungal strains and the resultant mycelial materials. We found that material generated from the deletion strain possessed larger hyphal diameter (Fig. 4), altered cell wall composition (Figs. 6 and 7), more densely packed hyphae (Fig. 3), and higher total biomass (Fig. 1). We speculate that the two latter phenotypes are most likely due to a significant reduction in developmental structures (i.e., conidiophores; Figs. 3 and 9) in the deletion mutant. This reduction in developmental structures appears to have allowed hyphae in the deletion mutant to grow more closely together, resulting in a material that was more closely packed, containing fewer voids. We speculate that this was the cause for the higher values of ultimate tensile strength. This finding is consistent with previous studies which have shown that mycelial materials with more densely packed hyphae have higher ultimate tensile strength [21]. However, to determine the specific impact of each of these different phenotypes (i.e., hyphal diameter, wall composition, developmental

structures, hyphal packing density) will require additional experiments.

Acknowledgements

We gratefully acknowledge significant assistance from personnel in the UMBC, Keith R. Porter Imaging Facility regarding SEM preparation and imaging; Drs. Michael Duffy and Joao Santos (Engineering Testing, LLC) for their assistance and guidance with material tensile testing; Dr. Govind Rao (UMBC, Center for Advanced Sensor Technology) for use of the laser cutter to prepare samples; Dr. Jorge Almodovar for general guidance with this project. We also thank the Electron Microscopy Core Imaging Facility at the University of Maryland, School of Medicine for their critical role with the entire TEM imaging process. Finally, we thank the UMBC, Molecular Characterization and Analysis Complex for use of the FTIR instrument.

Author contributions

KG helped lead conception of the work, designed and performed all experiments (except NMR work), analyzed all the data (except the NMR data), developed all the figures (except the NMR figures), wrote the entire manuscript (except for the NMR sections), and acquired funding for the project. HE, AGD, WH, and JL contributed significantly to the conception of the work. WP, NB, MEM, and SY assisted in the execution of experiments (except NMR work). IG performed the NMR work, conducted NMR analysis, developed the NMR figures and wrote the NMR section within the manuscript. SDH supervised the project, provided guidance throughout all phases of the project, edited the manuscript, and acquired funding for the project. MZ supervised and provided guidance throughout the mechanical testing portion of the project. MZ also provided the equipment used in the mechanical testing. TW supervised the entire NMR portion of the project, acquired funding, edited the manuscript and provided the equipment used for the NMR testing. TD trained KG on how to use the SEM, supervised SEM imaging, provided guidance for SEM preparation/design, and edited the manuscript. MRM first proposed the idea to me while I was an undergrad in college-inspiring me to come to UMBC and start my PhD journey here. MRM also supervised the project, provided guidance throughout all phases of the project, edited the manuscript, and acquired funding for the project.

Funding

Student support for this work was provided by an NIGMS Initiative for Maximizing Student Development (IMSD) Grant (5 R25 GM055036), an

NIGMS Graduate Research Training Initiative for Student Enhancement (G-RISE) Grant (T32-GM144876), G-RISE at UMBC awarded in 2021, National Science Foundation (NSF 2006189), and the Department of Defense (DoD) Science, Mathematics, and Research for Transformation (SMART) Scholarship - funded by the OUSD/R&E (The Under Secretary of Defense-Research and Engineering), and the National Defense Education Program (NDEP) / BA-1, Basic Research. The solid-state NMR analysis was supported by the National Institutes of Health (NIH) grant AI173270 to T.W.

Data availability

No datasets were generated or analysed during the current study.

Declarations

Competing interests

The authors declare no competing interests.

Author details

¹Department of Chemical, Biochemical and Environmental Engineering, University of Maryland, Baltimore County (UMBC), 1000 Hilltop Circle, Baltimore, MD 21250, USA

²Department of Plant Pathology, Entomology and Microbiology, Iowa State University, Ames, IA 50011, USA

³Department of Mechanical Engineering, University of Maryland, Baltimore County (UMBC), 1000 Hilltop Circle, Baltimore, MD 21250, USA

⁴Department of Chemistry, Michigan State University, 578 S. Shaw Ln, East Lansing, MI 48824, USA

⁵Keith R. Porter Imaging Facility, College of Natural and Mathematical Sciences, University of Maryland, Baltimore County (UMBC), 1000 Hilltop Circle, Baltimore, MD 21250, USA

Received: 26 September 2024 / Accepted: 30 November 2024

Published online: 18 December 2024

References

- Ramesh M, Palanikumar K, Reddy KH. Plant fibre based bio-composites: sustainable and renewable green materials. *Renew Sustain Energy Rev*. 2017;79:558–84.
- Nakhate P, Van Der Meer Y. A systematic review on seaweed functionality: a sustainable bio-based material. *Sustainability*. 2021;13(11):6174.
- Olivetti EA, Cullen JM. Toward a sustainable materials system. *Science*. 2018;360(6396):1396–8.
- Gawel E, Pannicke N, Hagemann N. A path transition towards a bioeconomy—the crucial role of sustainability. *Sustainability*. 2019;11(11):3005.
- Nations FAO/UN. Bioeconomy for a sustainable future. Food and Agriculture Organization of the United Nations; 2021.
- Babu KM. Silk from silkworms and spiders as high-performance fibers. *Structure and Properties of high-performance fibers*. Elsevier; 2017. pp. 327–66.
- Verma N, Jujjavarapu SE, Mahapatra C. Green sustainable biocomposites: substitute to plastics with innovative fungal mycelium based biomaterial. *J Environ Chem Eng*. 2023;11(5):110396.
- Abhijith R, Ashok A, Rejeesh CR. Sustainable packaging applications from mycelium to substitute polystyrene: a review. *Materials today: proceedings*. 2018;5(1):2139–45.
- Meyer V, Basenko EY, Benz JP, Braus GH, Caddick MX, Csukai M, et al. Growing a circular economy with fungal biotechnology: a white paper. *Fungal Biology Biotechnol*. 2020;7:5.
- Angelova GV, Brazkova MS, Krastanov AI. Renewable mycelium based composite – sustainable approach for lignocellulose waste recovery and alternative to synthetic materials – a review. 2021;76(11–12):431–42.
- Giometta C, Picco AM, Baiguera RM, Dondi D, Babbini S, Cartabia M, et al. Physico-mechanical and thermodynamic properties of mycelium-based biocomposites: a review. *Sustainability*. 2019;11(1):281.
- Alaneme KK, Anaele JU, Oke TM, Kareem SA, Adediran M, Ajibuwa OA, et al. Mycelium based composites: a review of their bio-fabrication procedures, material properties and potential for green building and construction applications. *Alexandria Eng J*. 2023;83:234–50.
- Vandeloek S, Elsacker E, Van Wylick A, De Laet L, Peeters E. Current state and future prospects of pure mycelium materials. *Fungal Biology Biotechnol*. 2021;8(1):1–10.
- Whabi V, Yu B, Xu J. From nature to design: tailoring pure Mycelial materials for the needs of tomorrow. *J Fungi*. 2024;10(3):183.
- Li K, Wei Z, Jia J, Xu Q, Liu H, Zhong C, et al. Engineered living materials grown from programmable aspergillus Niger mycelial pellets. *Mater Today Bio*. 2023;19:100545.
- Jo C, Zhang J, Tam JM, Church GM, Khalil AS, Segrè D, et al. Unlocking the magic in mycelium: using synthetic biology to optimize filamentous fungi for biomanufacturing and sustainability. *Mater Today Bio*. 2023;19:100560.
- Haneef M, Ceseracciu L, Canale C, Bayer IS, Heredia-Guerrero JA, Athanasios A. Advanced materials from fungal mycelium: fabrication and tuning of physical properties. *Sci Rep*. 2017;7(1):41292.
- Deeg K, Gima Z, Smith A, Stoica O, Tran K. Greener Solutions: Improving performance of mycelium-based leather. Final Report to MycoWorks. 2017:1–24.
- Appels FV, van den Brandhof JG, Dijksterhuis J, de Kort GW, Wösten HA. Fungal mycelium classified in different material families based on glycerol treatment. *Commun Biology*. 2020;3(1):1–5.
- Schaak D. inventor; Ecovative Design LLC., assignee. Bio-Manufacturing Process (Patent# 16/363052). United States of America 2019.
- Appels FVW, Dijksterhuis J, Lukasiewicz CE, Jansen KMB, Wösten HAB, Krijgsheld P. Hydrophobin gene deletion and environmental growth conditions impact mechanical properties of mycelium by affecting the density of the material. *Sci Rep*. 2018;8(1):4703.
- Gow NAR, Latge J-P, Munro CA. The fungal cell wall: structure, biosynthesis, and function. *Microbiol Spectr*. 2017;5(3):10–1128.
- Levin DE. Cell wall integrity signaling in *Saccharomyces cerevisiae*. *Microbiol Mol Biol Rev*. 2005;69(2):262–91.
- Fujioka T, Mizutani O, Furukawa K, Sato N, Yoshimi A, Yamagata Y, et al. MpkA-dependent and-independent cell wall integrity signaling in *aspergillus nidulans*. *Eukaryot Cell*. 2007;6(8):1497–510.
- Chelius CL, Ribeiro LF, Huso W, Kumar J, Lincoln S, Tran B, et al. Phosphoproteomic and transcriptomic analyses reveal multiple functions for *aspergillus nidulans* MpkA independent of cell wall stress. *Fungal Genet Biol*. 2019;125:1–12.
- De Souza CP, Hashmi SB, Osmani AH, Andrews P, Ringelberg CS, Dunlap JC, et al. Functional analysis of the *aspergillus nidulans* kinome. *PLoS ONE*. 2013;8(3):e58008.
- McCluskey K. The fungal genetics stock center. *Molds Molecules*. 2003;52:245–62.
- Nayak T, Szewczyk E, Oakley CE, Osmani A, Ukil L, Murray SL, et al. A versatile and efficient gene-targeting system for *aspergillus nidulans*. *Genetics*. 2006;172(3):1557–66.
- Harris SD, Morrell JL, Hamer JE. Identification and characterization of *aspergillus nidulans* mutants defective in cytokinesis. *Genetics*. 1994;136(2):517–32.
- Käfer E. Meiotic and mitotic recombination in *Aspergillus* and its chromosomal aberrations. *Adv Genet*. 1977;19:33–131.
- Sethi A, Kaur T, Malhotra SK, Gambhir ML. Moisturizers: the slippery road. *Indian J Dermatology*. 2016;61(3):279–87.
- Hamishkar H, Same S, Adibkia K, Zarza K, Shokri J, Taghaee M, et al. A comparative histological study on the skin occlusion performance of a cream made of solid lipid nanoparticles and Vaseline. *Res Pharm Sci*. 2015;10(5):378–87.
- Katti D, Krishnamurti N. Anionic polymerization of alkyl cyanoacrylates: in vitro model studies for in vivo applications. *J Appl Polym Sci*. 1999;74(2):336–44.
- Quintanilla D, Chelius C, Iambamung S, Nelson S, Thomas D, Gernaey KV, et al. A fast and simple method to estimate relative, hyphal tensile-strength of filamentous fungi used to assess the effect of autophagy. *Biotechnol Bioeng*. 2018;115(3):597–605.
- Chelius C, Huso W, Reese S, Doan A, Lincoln S, Lawson K, et al. Dynamic transcriptomic and phosphoproteomic analysis during cell wall stress in *aspergillus nidulans*. *Mol Cell Proteom*. 2020;19(8):1310–29.
- Lecellier A, Mounier J, Gaydou V, Castrec L, Barbier G, Ablain W, et al. Differentiation and identification of filamentous fungi by high-throughput FTIR spectroscopic analysis of mycelia. *Int J Food Microbiol*. 2014;168:32–41.
- Wilkerson RP. Biomimetic Nacre-Like, Metal-compliant-phase ceramics produced via Coextrusion. University of California, Berkeley; 2018.
- Li ZJ, Shukla V, Wenger K, Fordyce A, Pedersen AG, Marten M. Estimation of hyphal tensile strength in production-scale *aspergillus oryzae* fungal fermentations. *Biotechnol Bioeng*. 2002;77(6):601–13.

39. Vancleef A, Seurs S, Jordens J, Van Gerven T, Thomassen LCJ, Braeken L. Reducing the induction time using Ultrasound and High-Shear Mixing in a continuous crystallization process. *Cryst* [Internet]. 2018; 8(8).
40. Shirgaonkar IZ, Lothe RR, Pandit AB. Comments on the mechanism of microbial cell disruption in high-pressure and high-speed devices. *Biotechnol Prog*. 1998;14(4):657–60.
41. Latgé J-P, Wang T. Modern biophysics redefines our understanding of fungal cell wall structure, complexity, and dynamics. *Mbio*. 2022;13(3):e01145–22.
42. Latgé J-P, Chamilos G. *Aspergillus Fumigatus* and aspergillosis in 2019. *Clin Microbiol Rev*. 2019;33(1):10–1128.
43. Chakraborty A, Fernando LD, Fang W, Dickwella Widanage MC, Wei P, Jin C, et al. A molecular vision of fungal cell wall organization by functional genomics and solid-state NMR. *Nat Commun*. 2021;12(1):6346.
44. Kang X, Kirui A, Muszyński A, Widanage MCD, Chen A, Azadi P, et al. Molecular architecture of fungal cell walls revealed by solid-state NMR. *Nat Commun*. 2018;9(1):2747.
45. Dickwella Widanage MC, Gautam I, Sarkar D, Mentink-Vigier F, Vermaas JV, Ding S-Y, et al. Adaptive survival of *aspergillus fumigatus* to echinocandins arises from cell wall remodeling beyond $\beta - 1, 3$ -glucan synthesis inhibition. *Nat Commun*. 2024;15(1):6382.
46. Miyazawa K, Yoshimi A, Sano M, Tabata F, Sugahara A, Kasahara S, et al. Both galactosaminogalactan and α -1, 3-glucan contribute to aggregation of *aspergillus oryzae* hyphae in liquid culture. *Front Microbiol*. 2019;10:2090.
47. Nguyen PQ, Courchesne NMD, Duraj-Thatte A, Praveschotinunt P, Joshi NS. Engineered living materials: prospects and challenges for using biological systems to direct the assembly of smart materials. *Adv Mater*. 2018;30(19):1704847.
48. Alemu D, Tafesse M, Mondal AK. Mycelium-based composite: the future sustainable biomaterial. *Int J Biomaterials*. 2022;2022(1):8401528.
49. Adams TH, Timberlake WE. Developmental repression of growth and gene expression in *Aspergillus*. *Proceedings of the National Academy of Sciences*. 1990;87(14):5405-9.
50. Adams TH, Wieser JK, Yu J-H. Asexual sporulation in *aspergillus nidulans*. *Microbiol Mol Biol Rev*. 1998;62(1):35–54.
51. Mirabito PM, Adams TH, Timberlake WE. Interactions of three sequentially expressed genes control temporal and spatial specificity in *Aspergillus* development. *Cell*. 1989;57(5):859–68.
52. Perakis F, De Marco L, Shalit A, Tang F, Kann ZR, Kühne TD, et al. Vibrational spectroscopy and dynamics of water. *Chem Rev*. 2016;116(13):7590–607.
53. Eisenberg D, Kauzmann W. *The structure and properties of water*. Oxford University Press, USA; 2005.

Publisher's note

Springer Nature remains neutral with regard to jurisdictional claims in published maps and institutional affiliations.